Liquid boundary effect on free vibration of an annular plate coupled with a liquid

Kyeong-Hoon Jeong*

*SMART System Development Division, Korea Atomic Energy Research Institute,
111 Daedeok-daero 989 Beon-gil, Yuseong, Daejeon, 34057, Republic of Korea*

Abstract. A theoretical method is developed to analyze the free vibration of an elastic annular plate in contact with an ideal liquid. The displacement potential functions of the contained liquid are expressed as a combination of the Bessel functions that satisfy the Laplace equation and the liquid boundary conditions. The compatibility condition along the interface between the annular plate and the contained liquid is taken into account to consider the fluid-structure coupling. The dynamic displacement of the wet annular plate is assumed to be a combination of dry eigenfunctions, allowing for prediction of the natural frequencies using the Rayleigh-Ritz method. The study investigates the effect of radial liquid boundary conditions on the natural frequencies of the wet annular plate, considering four types of liquid bounding: outer container bounded, outer and inner bounded, inner bounded, and radially unbounded. The proposed theoretical method is validated by comparing the predicted wet natural frequencies with those obtained from finite element analysis, showing excellent accuracy. The results indicate that the radial liquid bounding effect on the natural frequencies is negligible for the axisymmetric vibrational mode, but relatively significant for the mode with one nodal diameter ($n = 1$) and no nodal circle ($m' = 0$). Furthermore, the study reveals that the wet natural frequencies are the largest for the plate with an inner bounded cylinder among the radial liquid boundary cases, regardless of the vibration mode.

Keywords: annular plate; Hankel transform; hydrodynamic mass; hydroelastic vibration; liquid-contacting; radial liquid boundary

1. Introduction

The effect of liquid inertia on free vibration of structures coupled with a liquid are commonly characterized by the added mass or hydrodynamic mass, as noted by Chen *et al.* (2021), Lin *et al.* (2022), Wang *et al.* (2019), Zhang *et al.* (2022). The presence of liquid tends to reduce the natural frequencies of the liquid-coupled system. Annular type plates are widely used in engineering, and their dynamics in contact with a liquid have been investigated through analytical and experimental studies. In particular, the dynamics of annular plates in contact with a liquid have been investigated both analytically and experimentally. For instance, the bottom plates of a small nuclear reactor consist of multiple annular plates submerged in coolant, which are designed to mitigate radiation

---

*Corresponding author, Ph.D., E-mail: khjeong@kaeri.re.kr

from the core to the reactor pressure vessel outside. The presence of coolant between the annular plates can be radially bounded or not, and it is important to investigate the effect of coolant bounding on the dynamic characteristics of the bottom plates.

As a result, numerous studies on the free vibration of annular plates or circular plates in contact with a liquid have been published. Amabili (1996) theoretically studied the free vibration of annular plates coupled with an ideal liquid with a finite depth using the Rayleigh-Ritz method with assumed vibrational modes. In the paper, the liquid domain was assumed to be unbounded in the radial direction, but the top of the liquid had either a free surface or was bounded by a rigid cover. Amabili *et al.* (1996) suggested an analytical method to obtain wet natural frequencies of liquid-contacting annular plates fixed along an infinite rigid wall using the Hankel transform. Bauer and Komatsu (2000) studied the hydroelastic vibration of a liquid-contacting flexible annular plate supported by two rigid cylindrical containers. A theory on the natural frequencies of free-edge annular plates (Kwak and Amabili 1999, Liang *et al.* 1999) and circular plates (Kwak and Han 2000) resting on a free surface or completely submerged was developed employing the Hankel transform. Modal tests were also carried out for free-edge annular plates to determine the non-dimensionalized added virtual mass incremental (NAVMI) factors. Jeong *et al.* (2005) developed an analytical method for free vibration of a circular plate submerged in a bounded compressible liquid using the Rayleigh-Ritz method based on the Fourier-Bessel series expansion, and found that the liquid compressibility and off-center distance of the plate in the liquid storage cylindrical tank significantly affect the wet natural frequencies. Jeong (2006) presented a theoretical study on the hydroelastic vibration of two annular plates coupled with a bounded liquid using the finite Hankel transform. Kim and Lee (2005) analytically investigated the structural and sloshing modes of an elastic annular plate fixed on a liquid-filled rigid cylindrical storage tank, taking into account the free surface effect of the liquid in the theory. Askari *et al.* (2013) developed a theoretical method to investigate free vibrations of a circular plate immersed in a liquid, where the coupled governing equations of both the hydroelastic vibration of the plate and liquid sloshing were simultaneously solved by a semi-analytical procedure. The proposed approach was verified by both modal tests and finite element analyses for circular steel plates submerged in a container filled with water. Escaler *et al.* (2018) performed experimental and numerical analyses to determine the effects of water loading on the axisymmetric modes of vibration of a fully submerged circular plate. Recently, Askari *et al.* (2020) theoretically studied the dynamics of an eccentric annular plate in contact with a fluid, and Hosseini (2017) suggested a suspended submerged annular plate as a sloshing reduction tool in oil storage tanks. In the above studies on annular plates or circular plates, it was possible to obtain a solution using integral transformations such as the Hankel transform with the Rayleigh-Ritz method.

However, the major concern in previous studies was the effect of the liquid depth on the natural frequencies of the liquid-contacting plates, and investigation on the effect of the radial liquid boundary condition on free vibration of circular or annular plates was rare. Therefore, this study develops theoretical formulations for a flexible annular plate in contact with an ideal liquid with various radial liquid boundary conditions, and investigates the effect of the radial constraints of the liquid on the wet natural frequencies of the liquid-contacting annular plate. The theoretical approach for several radial liquid boundaries is verified using finite element analyses.

2. Theoretical formulation

2.1 Description of annular plate coupled with liquid

(a) Outer bounded case (Case A)

(b) Outer and inner bounded case (Case B)

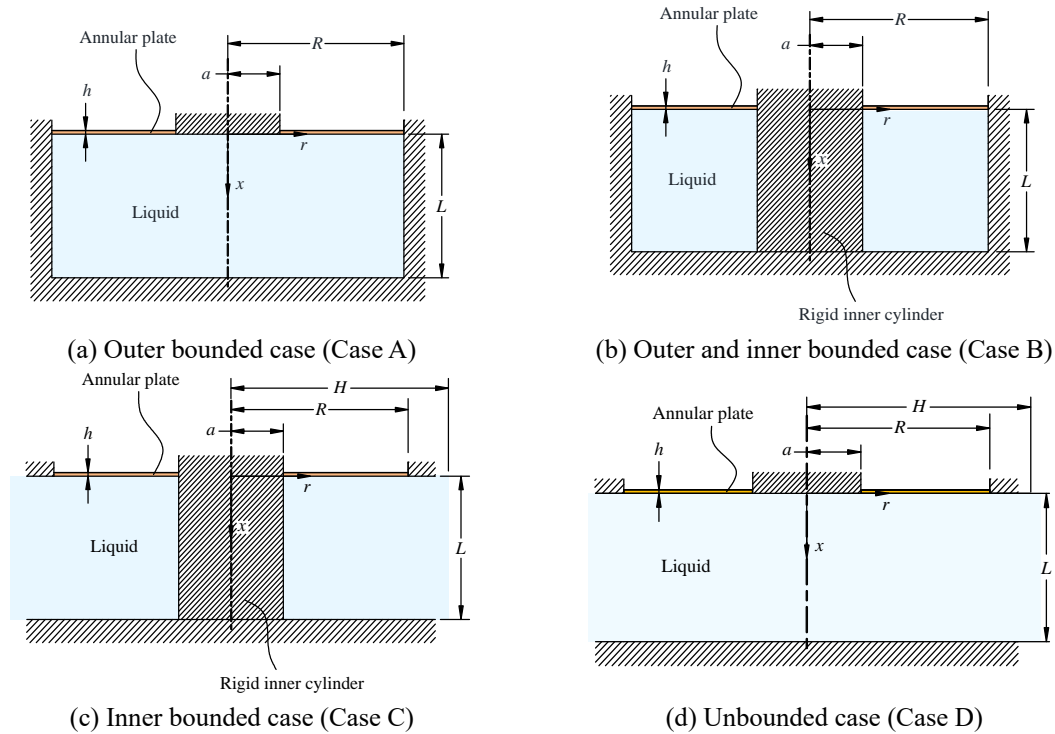(c) Inner bounded case (Case C)

(d) Unbounded case (Case D)

Fig. 1 Mathematical model of an annular plate coupled with a liquid

Theoretical models for a flexible annular plate in contact with an ideal liquid are illustrated in Fig. 1. Four cases of the radial liquid boundary condition are taken into consideration in the analysis: Case A shows that the contained liquid is radially bounded by the outer rigid container only; Case B illustrates that the contained liquid is radially bounded by both the inner rigid cylinder and outer rigid container; Case C demonstrates that the liquid is radially bounded by the inner rigid cylinder only, but it is radially unbounded along the outer liquid edge; Case D describes that the liquid is totally unbounded in the radial direction. It is assumed that the homogeneous elastic annular plate with the thickness h is clamped along both the inner and outer edges with the inner radius a and outer radius R. The cylindrical inner rigid cylinder, the outer container, and the outer liquid edge have the radius a, R, and H, respectively, as shown in Fig. 1. The radially unbounded cases such as Cases C and D can be simulated by applying a significantly large radius of the outer edge with zero liquid displacement potential. The contained liquid with a depth L is bounded axially by a rigid bottom.

2.2 Equation of motion for dry annular plate

Assuming small deformations, the partial differential equation of motion for the transverse displacement, w, of the annular plate is given by Eq. (1) in the polar coordinate system (r, θ) (Jeong *et al.* 2005, Kwak and Amabili 1999).

$$D\nabla^4 w(r,\theta,t) + \rho\, \partial^2 w / \partial t^2 = p(r,\theta,t) \tag{1}$$

where, $p(r,\theta,t)$ is the oscillating hydrodynamic pressure exerted on the plate, *t* time, and ρ the mass density of the annular plate per unit area. The oscillating hydrodyanmic pressure on the plate in the dry condition is definitley zero. The flexural rigidity of the plate in Eq. (1) is defined as $D = Eh^3 / 12(1-\mu^2)$, where the modulus of elasticity and the Poisson's ratio of the plate are indicated by *E* and μ, respectively. The transverse dynamic displacement of the annular plate *w*, regardless of the liquid presence, is written as Eq. (2).

$$w(r,\theta,t) = \sum_{m=1}^{M} q_{nm} W_m(r,\theta) \exp(i\omega t) \tag{2}$$

where $i = \sqrt{-1}$, and ω is the natural frequency of the annular plate. Each mode shape of the annular plate can be expanded using a finite number of displacement modal functions, denoted by $W_m(r,\theta)$, and the unknown coefficient, q_{nm}, for dynamic deformation of the flexible annular plate. The function $W_m(r,\theta)$ in Eq. (2) is assumed to be the *m*-th eigen-function of the dry annular plate which satisfies the boundary condition along both the edges for a fixed wave number *n*. The wave number *n* also indicates the number of nodal diameters in the vibration mode (Jeong 2006).

$$W_m(r,\theta) = \bar{W}_{nm}(r) \cos(n\theta) \tag{3}$$

$$\bar{W}_{nm}(r) = J_n(\lambda_{nm} r) + C_{nm1} Y_n(\lambda_{nm} r) + C_{nm2} I_n(\lambda_{nm} r) + C_{nm3} K_n(\lambda_{nm} r) \tag{4}$$

in which J_n and Y_n are the Bessel functions of the first and second kinds, and I_n and K_n are the the modified Bessel functions of the first and second kinds, respectively. The frequency parameter is denoted by λ_{mn} in Eq. (4). Furthermore, *m* of Eq. (4) represents the number of expanding terms for the radial modal function. The unknown coefficients, C_{nmj} (*j* =1, 2, 3) in Eq. (4) are determined by the boundary conditions along the inner and outer edges of the annular plate. Before determining the natural frequencies of the liquid-structure coupled system, the clamped boundary conditions must be satisfied in conjunction with the plate displacement and slope, that is, $\bar{W}_{nm} = 0$ and $d\bar{W}_{nm} / dr = 0$ at *r=R* and *r=a*. Therefore, the frequency parameter for the dry clamped annular plate can be obtained by Eq. (5).

$$\begin{vmatrix} J_n(\lambda_{nm} a) & Y_n(\lambda_{nm} a) & I_n(\lambda_{nm} a) & K_n(\lambda_{nm} a) \\ J_n(\lambda_{nm} R) & Y_n(\lambda_{nm} R) & I_n(\lambda_{nm} R) & K_n(\lambda_{nm} R) \\ J_n'(\lambda_{nm} a) & Y_n'(\lambda_{nm} a) & I_n'(\lambda_{nm} a) & K_n'(\lambda_{nm} a) \\ J_n'(\lambda_{nm} R) & Y_n'(\lambda_{nm} R) & I_n'(\lambda_{nm} R) & K_n'(\lambda_{nm} R) \end{vmatrix} = 0 \tag{5}$$

where, the prime (') indicates the derivative of the Bessel functions with respect to *r*. For the clamped annular plate along the inner and outer edges, the modal coefficients C_{nmj} (*j* =1, 2, 3) in Eq. (4) can be derived as listed in Appendix (Jeong 2006). The natural frequencies of the clamped dry annular plate, ω_a are obtained using Eqs. (5) and (6).

$$\omega_a = \lambda_{nm}^2 \sqrt{D/\rho} \tag{6}$$

2.3 Liquid motion

2.3.1 Displacement potential function of liquid

The motion of the liquid in contact with the annular plate can be described using the displacement potential function that satisfies the Laplace equation in the cylindrical coordinates under the assumption of an ideal liquid.

$$\nabla^2 \Phi (r, \theta, x, t) = 0 \tag{7}$$

The displacement potential function of the contained liquid, Φ can be separated into two spatial displacement potential functions, $\phi_{ns}(r)$ and $\eta_{ns}(x)$ with the harmonic time function (Kwak and Amabili 1999).

$$\Phi(r, \theta, x, t) = \sum_{s=1}^{\infty} \phi_{ns}(r)\, \eta_{ns}(x) \cos(n\theta) \exp(\mathrm{i}\,\omega\, t) \tag{8}$$

The general solution of Eq. (7) for a fixed circumferential wave number, n is given by the combination in multiplication of the radial and axial displacement potential functions as delineated in Eq. (8). The radial and axial displacement potential functions of Eq. (8) can be expressed by the Bessel and hyperbolic sinusoidal functions, respectively.

$$\phi_{ns}(r) = A_{ns1}\, \mathrm{J}_n(\beta_{ns}\, r) + A_{ns2}\, \mathrm{Y}_n(\beta_{ns}\, r) \tag{9}$$

$$\eta_{ns}(x) = \sinh(\beta_{ns}\, x) + B_{ns} \cosh(\beta_{ns}\, x) \tag{10}$$

The liquid boundary condition at the impermeable rigid bottom wall satisfies Eq. (11), and it leads to Eq. (12).

$$d\eta_{ns}(x)/dx\big]_{x=L} = 0 \tag{11}$$

$$\eta_{ns}(x) = \sinh(\beta_{ns}\, x) - \cosh(\beta_{ns}\, x)/\tanh(\beta_{ns}\, L) \tag{12}$$

2.3.2 Radial displacement potential function of Case A

As the radial displacement potential function of the liquid for Case A should be finite at $r = 0$, the term of the second kind of Bessel function, Y_n in Eq. (9) vanishes. So, the displacement potential function of Eq. (9) is simplified to Eq. (13).

$$\phi_{ns}(r) = A_{ns1}\, \mathrm{J}_n(\beta_{ns}\, r) \tag{13}$$

In addition, the liquid boundary condition at the impermeable rigid container wall should satisfy the equation.

$$d\phi_{ns}(r)/dr\big|_{r=R} = 0 \tag{14}$$

Substituting Eq. (13) into Eq. (14) leads to the transcendental equation.

$$\mathrm{J}_n'(\beta_{ns}\, R) = 0 \tag{15}$$

in which, the coefficients, β_{ns} in Eq. (13) are determined by Eq. (15) for each nodal diameter, n.

2.3.3 Radial displacement potential function of Case B

The impermeable condition along both the rigid outer container and the inner cylinder for Case B implies

$$d\phi_{ns}(r)/dr\big|_{r=R}=0 \tag{16}$$

$$d\phi_{ns}(r)/dr\big|_{r=a}=0 \tag{17}$$

The radial displacement potential function for Case B that satisfies Eq. (16) is given as Eq. (18).

$$\phi_{ns}(r)=A_{ns1}\left[Y_n{}'(\beta_{ns}R)J_n(\beta_{ns}r)-J_n{}'(\beta_{ns}R)Y_n(\beta_{ns}r)\right] \tag{18}$$

By substituting Eq. (18) into Eq. (17), we can obtain the transcendental equation of Eq. (19). Therefore, the coefficients, β_{ns} in Eq. (18) are obtained by Eq. (19) for Case B.

$$J_n{}'(\beta_{ns}a)Y_n{}'(\beta_{ns}R)-J_n{}'(\beta_{ns}R)Y_n{}'(\beta_{ns}a)=0 \tag{19}$$

2.3.4 Radial displacement potential function of Case C

As the radial displacement potential function for Case C can be similarly determined by the boundary condition of Eq. (20) along the impermeable inner rigid cylindrical wall and the boundary condition of Eq. (21) along the liquid edge for $H(>>R)$.

$$d\phi_{ns}(r)/dr\big|_{r=a}=0 \tag{20}$$

$$\phi_{ns}(r)\big|_{r=H}=0 \tag{21}$$

The displacement potential function of the radial direction satisfying the Laplace equation of Eq. (7) and Eq. (21) is written as

$$\phi_{ns}(r)=A_{ns1}\left\{Y_n(\beta_{ns}H)J_n(\beta_{ns}r)-J_n(\beta_{ns}H)Y_n(\beta_{ns}r)\right\} \tag{22}$$

Therefore, the transcendental equation of Eq. (23) can be derived by substituting Eq. (22) into Eq. (20).

$$Y_n(\beta_{ns}H)J_n{}'(\beta_{ns}a)-J_n(\beta_{ns}H)Y_n{}'(\beta_{ns}a)=0 \tag{23}$$

The coefficients, β_{ns} of Eq. (22) for Case C are extracted using Eq. (23) for each circumferential wave number, n.

2.3.5 Radial displacement potential function of Case D

The liquid displacement potential function for Case D can be similarly determined by the boundary condition of Eq. (21) along the liquid edge. As the liquid displacement potential function for Case D must be finite at $r=0$, the displacement potential function of Eq. (9) is reduced to Eq. (13) for $H>>R$. Inserting Eq. (13) into Eq. (21) gives

$$J_n(\beta_{ns}H)=0 \tag{24}$$

where, the coefficients, β_{ns}, for Case D are calculated by the transcendental equation of Eq. (24).

2.4 Compatibility condition

2.4.1 Liquid-plate interaction

When the bottom surface of the annular plate must remain in contact with the liquid during its oscillation, the axial compatibility condition along the liquid interfacing surface with the annular

plate yields

$$w(r,\theta,t) = \left[\partial \Phi(r,\theta,x,t) / \partial x \right]_{x=0} \quad \text{for } a \le r \le R \tag{25}$$

Therefore, Eq. (25) is converted to Eq. (26) by replacing Eqs. (2), (3), and (8) into Eq. (25).

$$\sum_{m=1}^{M} q_{nm} W_m(r,\theta) = \sum_{m=1}^{M} q_{nm} \bar{W}_{nm}(r) \cos(n\theta) = \sum_{s=1}^{\infty} \phi_{ns}(r) \left(d\eta_{ns}(x) / dx \big|_{x=0} \right) \cos(n\theta) \tag{26}$$

Inserting Eqs. (4) and (12) into Eq. (26) gives

$$\sum_{m=1}^{M} q_{nm} \left[J_n(\lambda_{nm} r) + C_{nm1} Y_n(\lambda_{nm} r) + C_{nm2} I_n(\lambda_{nm} r) + C_{nm3} K_n(\lambda_{nm} r) \right] = \sum_{s=1}^{\infty} \beta_{ns} \phi_{ns}(r) \tag{27}$$

2.4.2 Displacement potential function of Case A

The compatibility condition for Case A is revealed from Eqs. (27) and (13).

$$\sum_{m=1}^{M} q_{nm} \left[J_n(\lambda_{nm} r) + C_{nm1} Y_n(\lambda_{nm} r) + C_{nm2} I_n(\lambda_{nm} r) + C_{nm3} K_n(\lambda_{nm} r) \right] = \sum_{s=1}^{\infty} A_{ns1} \beta_{ns} J_n(\beta_{ns} r) \tag{28}$$

Eq. (28) is modified to Eq. (29) for $n=0$, since the coefficient, $\beta_{ns} = 0$ when $s=1$.

$$\sum_{m=1}^{M} q_{0m} \left[J_0(\lambda_{0m} r) + C_{0m1} Y_0(\lambda_{0m} r) + C_{0m2} I_0(\lambda_{0m} r) + C_{0m3} K_0(\lambda_{0m} r) \right] = \sum_{s=2}^{\infty} A_{0s1} \beta_{0s} J_0(\beta_{0s} r) \tag{29}$$

For $n=0$ of Case A, hereinafter Eq. (29) is applied instead of Eq. (28). The finite Henkel transformation is applied to Eq. (28) to obtain a relation between the coefficients for the liquid and plate motions. As a result, Eq. (28) is developed into Eq. (30) by integration along the interval $(0, R)$ after multiplication of weighting function, $r J_n(\beta_{ns} r)$.

$$\sum_{m=1}^{M} q_{nm} \sum_{s=1}^{\infty} \int_a^R r J_n(\beta_{ns} r) \left[J_n(\lambda_{nm} r) + C_{nm1} Y_n(\lambda_{nm} r) + C_{nm2} I_n(\lambda_{nm} r) + C_{nm3} K_n(\lambda_{nm} r) \right] dr$$

$$= \sum_{s=1}^{\infty} A_{ns1} \beta_{ns} \int_0^R r \left\{ J_n(\beta_{ns} r) \right\}^2 dr \tag{30}$$

Eq. (30) can be rewritten as Eq. (31) based on the orthogonal property of the Bessel function, $J_n(\beta_{ns} r)$.

$$\sum_{m=1}^{M} q_{nm} \sum_{s=1}^{\infty} \left(\Gamma_{nms1} + C_{nm1} \Gamma_{nms2} + C_{nm2} \Gamma_{nms3} + C_{nm3} \Gamma_{nms4} \right) = \sum_{s=1}^{\infty} A_{ns1} \beta_{ns} K_{ns} \tag{31}$$

The integral coefficients, Γ_{nms1}, Γ_{nms2}, Γ_{nms3}, Γ_{nms4}, and K_{ns} in Eq. (31) are defined in Appendix. The coefficient for liquid motion, A_{ns1}, can be briefly written in terms of the unknown coefficient for dynamic displacement of the plate, q_{nm}.

$$A_{ns1} = \left[\beta_{ns} K_{ns} \right]^{-1} \sum_{m=1}^{M} q_{nm} \Psi_{nms} \tag{32}$$

$$\Psi_{nms} = \left(\Gamma_{nms1} + C_{nm1} \Gamma_{nms2} + C_{nm2} \Gamma_{nms3} + C_{nm3} \Gamma_{nms4} \right) \tag{33}$$

The radial displacement potential function, $\phi_{ns}(r)$, for Case A is finally given as

$$\phi_{ns}(r) = [\beta_{ns} K_{ns}]^{-1} \sum_{m=1}^{M} q_{nm} \Psi_{nms} J_n(\beta_{ns} r) \tag{34}$$

2.4.3 Displacement potential of Case B

The compatibility condition for Case B is redefined by substituting Eq. (18) into Eq. (27).

$$\sum_{m=1}^{M} q_{nm} \left[J_n(\lambda_{nm} r) + C_{nm1} Y_n(\lambda_{nm} r) + C_{nm2} I_n(\lambda_{nm} r) + C_{nm3} K_n(\lambda_{nm} r) \right]$$

$$= \sum_{s=1}^{\infty} \beta_{ns} A_{ns1} \left[Y_n'(\beta_{ns} R) J_n(\beta_{ns} r) - J_n'(\beta_{ns} R) Y_n(\beta_{ns} r) \right] \tag{35}$$

A finite Henkel transformation of Eq. (35) is applied to obtain a relation between the unknown coefficients for the liquid and plate motions. Therefore, Eq. (35) is transformed into Eq. (36) by integration along the radial interval (*a, R*) after multiplication of a weighting function, $r \left[Y_n'(\beta_{ns} R) J_n(\beta_{ns} r) - J_n'(\beta_{ns} R) Y_n(\beta_{ns} r) \right]$.

$$\sum_{m=1}^{M} q_{nm} \sum_{s=1}^{\infty} \int_a^R r \left[Y_n'(\beta_{ns} R) J_n(\beta_{ns} r) - J_n'(\beta_{ns} R) Y_n(\beta_{ns} r) \right] \left[J_n(\lambda_{nm} r) + C_{nm1} Y_n(\lambda_{nm} r) \right.$$

$$\left. + C_{nm2} I_n(\lambda_{nm} r) + C_{nm3} K_n(\lambda_{nm} r) \right] dr = \sum_{s=1}^{\infty} \int_a^R \beta_{ns} A_{ns1} r \left[Y_n'(\beta_{ns} R) J_n(\beta_{ns} r) \right.$$

$$\left. - J_n'(\beta_{ns} R) Y_n(\beta_{ns} r) \right]^2 dr \tag{36}$$

The coefficient for the liquid motion, A_{ns1}, in Eq. (36) can be written as a variable of the unknown coefficient for the plate, q_{nm}, based on the orthogonal property for the weighting function.

$$A_{ns1} = [\beta_{ns} G_{ns}]^{-1} \sum_{m=1}^{M} q_{nm} \Theta_{nms} \tag{37}$$

$$\Theta_{nms} = \left(\Lambda_{nms1} + C_{nm1} \Lambda_{nms2} + C_{nm2} \Lambda_{nms3} + C_{nm3} \Lambda_{nms4} \right) \tag{38}$$

The integral coefficients, Λ_{nms1}, Λ_{nms2}, Λ_{nms3}, Λ_{nms4}, and G_{ns} in Eqs. (37) and (38) are defined in Appendix, and the radial displacement potential function, $\phi_{ns}(r)$ for Case B can be explicitly expressed as

$$\phi_{ns}(r) = [\beta_{ns} G_{ns}]^{-1} \sum_{m=1}^{M} q_{nm} \Theta_{nms} \left[Y_n'(\beta_{ns} R) J_n(\beta_{ns} r) - J_n'(\beta_{ns} R) Y_n(\beta_{ns} r) \right] \tag{39}$$

2.4.4 Displacement potential function of Case C

The compatibility condition for Case C is given by inserting Eq. (22) into Eq. (27).

$$\sum_{m=1}^{M} q_{nm} \left[J_n(\lambda_{nm} r) + C_{nm1} Y_n(\lambda_{nm} r) + C_{nm2} I_n(\lambda_{nm} r) + C_{nm3} K_n(\lambda_{nm} r) \right] = \sum_{s=1}^{\infty} \beta_{ns} A_{ns1} \{ Y_n(\beta_{ns} H) J_n(\beta_{ns} r)$$

$$- J_n(\beta_{ns} H) Y_n(\beta_{ns} r) \} \tag{40}$$

Performing an integration in the liquid interval (a, H) after multiplication of $r\left\{Y_n(\beta_{ns}H)J_n(\beta_{ns}r)-J_n(\beta_{ns}H)Y_n(\beta_{ns}r)\right\}$ to Eq. (40) leads to

$$\sum_{m=1}^{M}q_{nm}\sum_{s=1}^{\infty}\int_{a}^{R}r\left\{Y_n(\beta_{ns}H)J_n(\beta_{ns}r)-J_n(\beta_{ns}H)Y_n(\beta_{ns}r)\right\}$$

$$\times\left[J_n(\lambda_{nm}r)+C_{nm1}Y_n(\lambda_{nm}r)+C_{nm2}I_n(\lambda_{nm}r)+C_{nm3}K_n(\lambda_{nm}r)\right]dr$$

$$=\sum_{s=1}^{\infty}\int_{a}^{H}\beta_{ns}A_{ns1}r\left\{Y_n(\beta_{ns}H)J_n(\beta_{ns}r)-J_n(\beta_{ns}H)Y_n(\beta_{ns}r)\right\}^2dr \qquad (41)$$

The coefficient of the liquid motion, A_{ns1}, for Case C can be similarly expressed in terms of the unknown coefficient of the plate, q_{nm}, as briefly delineated in Eqs. (42) and (43).

$$A_{ns1}=\left[\beta_{ns}F_{ns}\right]^{-1}\sum_{m=1}^{M}q_{nm}\,\Pi_{nms} \qquad (42)$$

$$\Pi_{nms}=\left(\Xi_{nms1}+C_{nm1}\Xi_{nms2}+C_{nm2}\Xi_{nms3}+C_{nm3}\Xi_{nms4}\right) \qquad (43)$$

The integral coefficients, Ξ_{nms1}, Ξ_{nms2}, Ξ_{nms3}, Ξ_{nms4}, and F_{ns} in Eqs. (42) and (43) are defined in Appendix, and the radial displacement potential function for the liquid, $\phi_{ns}(r)$ for Case C is given by

$$\phi_{ns}(r)=\left[\beta_{ns}F_{ns}\right]^{-1}\sum_{m=1}^{M}q_{nm}\,\Pi_{nms}\left[Y_n(\beta_{ns}H)J_n(\beta_{ns}r)-J_n(\beta_{ns}H)Y_n(\beta_{ns}r)\right] \qquad (44)$$

2.4.5 Displacement potential function of Case D
The compatibility condition for Case D is given by inserting Eq. (13) into Eq. (27).

$$\sum_{m=1}^{M}q_{nm}\left[J_n(\lambda_{nm}r)+C_{nm1}Y_n(\lambda_{nm}r)+C_{nm2}I_n(\lambda_{nm}r)+C_{nm3}K_n(\lambda_{nm}r)\right]=\sum_{s=1}^{\infty}\beta_{ns}A_{ns1}J_n(\beta_{ns}r) \qquad (45)$$

Performing an integration in the liquid interval (0, H) after multiplying by $rJ_n(\beta_{ns}r)$ to Eq. (45) results in

$$\sum_{m=1}^{M}q_{nm}\sum_{s=1}^{\infty}\int_{a}^{R}rJ_n(\beta_{ns}r)\left[J_n(\lambda_{nm}r)+C_{nm1}Y_n(\lambda_{nm}r)+C_{nm2}I_n(\lambda_{nm}r)+C_{nm3}K_n(\lambda_{nm}r)\right]dr$$

$$=\sum_{s=1}^{\infty}\int_{0}^{H}\beta_{ns}A_{ns1}r\left\{J_n(\beta_{ns}r)\right\}^2dr \qquad (46)$$

The coefficient of liquid motion, A_{ns1} for Case D can be similarly written in the unknown coefficient for plate, q_{nm} as briefly given in Eqs. (47) and (48).

$$A_{ns1}=\frac{1}{\beta_{ns}Q_{ns}}\sum_{m=1}^{M}q_{nm}\,\Delta_{nms} \qquad (47)$$

$$\Delta_{nms}=\left(\Omega_{nms1}+C_{nm1}\Omega_{nms2}+C_{nm2}\Omega_{nms3}+C_{nm3}\Omega_{nms4}\right) \qquad (48)$$

The integral coefficients, Ω_{nms1}, Ω_{nms2}, Ω_{nms3}, Ω_{nms4}, and Q_{ns} in Eqs. (47) and (48) are defined in Appendix, and the radial displacement potential function, $\phi_{ns}(r)$ for Case D is finally written as

$$\phi_{ns}(r) = [\beta_{ns} Q_{ns}]^{-1} \sum_{m=1}^{M} q_{nm} \Lambda_{nms} J_n(\beta_{ns} r) \tag{49}$$

3. Method of solution

3.1 Kinetic energy of liquid

The natural frequencies of an annular plate can be estimated by the ratio of the potential energy and to kinetic energy of the system. The natural frequencies, ω_a in the dry condition, and ω in the wet condition are given by the Rayleigh quotient, respectively.

$$\omega_a^2 = V_p / T_p^* \quad \text{for the dry condition} \tag{50}$$

$$\omega^2 = V_p / (T_p^* + U_F^*) \quad \text{for the wet condition} \tag{51}$$

where, V_p and T_p^* represent the maximum potential and reference kinetic energies of the vibrating annular plate, respectively. The reference kinetic energy of the liquid, U_F^* in Eq. (51) can be evaluated by its integration along the wet surface of the annular plate.

$$U_F^* = -\frac{1}{2} \rho_o \kappa_\theta \int_a^R r \sum_{k=1}^{M} \bar{W}_{nk}(r) \sum_{s=1}^{\infty} \phi_{ns}(r) [\eta_{ns}(x)]_{x=0} \, dr \tag{52}$$

where ρ_o is the mass density of the liquid, and

$$\kappa_\theta = \begin{bmatrix} 2\pi & \text{for} & n = 0 \\ \pi & \text{for} & n > 0 \end{bmatrix} \tag{53}$$

$$[\eta_{ns}(x)]_{x=0} = -[\tanh(\beta_{ns} L)]^{-1} \tag{54}$$

The reference liquid kinetic energy, U_F^* of Eq. (52) for Case A takes the following form by substituting Eqs. (4) and (34) into Eq. (52).

$$U_F^* = \frac{1}{2} \rho_o \kappa_\theta \sum_{s=1}^{\infty} \sum_{k=1}^{M} \left\{ \int_a^R r \left[J_n(\lambda_{nk} r) + C_{nk1} Y_n(\lambda_{nk} r) + C_{nk2} I_n(\lambda_{nk} r) + C_{nk3} K_n(\lambda_{nk} r) \right] \right.$$
$$\left. \times [\beta_{ns} \tanh(\beta_{ns} L) K_{ns}]^{-1} \sum_{m=1}^{M} q_{nm} \Psi_{nms} J_n(\beta_{ns} r) \, dr \right\} \tag{55}$$

Therefore, it is represented as a reduced form.

$$U_F^* = \frac{1}{2} \rho_o \kappa_\theta \sum_{s=1}^{\infty} \frac{1}{\beta_{ns} \tanh(\beta_{ns} L) K_{ns}} \sum_{k=1}^{M} q_{nk} \Psi_{nks} \sum_{m=1}^{M} q_{nm} \Psi_{nms} \tag{56}$$

For Case B, the reference kinetic energy of the liquid, U_F^* in Eq. (52) similarly becomes

$$U_F^* = \frac{1}{2}\rho_o\,\kappa_\theta \sum_{s=1}^{\infty}\sum_{k=1}^{M}\left\{\int_a^R r\left[J_n\left(\lambda_{nk}\,r\right) + C_{nk1}\,Y_n\left(\lambda_{nk}\,r\right) + C_{nk2}\,I_n\left(\lambda_{nk}\,r\right) + C_{nk3}\,K_n\left(\lambda_{nk}\,r\right)\right]\right.$$

$$\left. \times\left[\beta_{ns}\tanh\left(\beta_{ns}\,L\right)G_{ns}\right]^{-1}\sum_{m=1}^{M}q_{nm}\,\Theta_{nms}\left[Y_n{}'\left(\beta_{ns}\,R\right)J_n\left(\beta_{ns}\,r\right) - J_n{}'\left(\beta_{ns}\,R\right)Y_n\left(\beta_{ns}\,r\right)\right]dr\right\} \tag{57}$$

Eq. (57) is reduced to a simple expression.

$$U_F^* = \frac{1}{2}\rho_o\,\kappa_\theta \sum_{s=1}^{\infty}\left[\beta_{ns}\tanh\left(\beta_{ns}\,L\right)G_{ns}\right]^{-1}\sum_{k=1}^{M}q_{nk}\,\Theta_{nks}\sum_{m=1}^{M}q_{nm}\,\Theta_{nms} \tag{58}$$

For Case C, the reference liquid kinetic energy, U_F^* in Eq. (52) is also similarly written

$$U_F^* = \frac{1}{2}\rho_o\,\kappa_\theta \sum_{s=1}^{\infty}\sum_{k=1}^{M}\left\{\int_a^R r\left[J_n\left(\lambda_{nk}\,r\right) + C_{nk1}\,Y_n\left(\lambda_{nk}\,r\right) + C_{nk2}\,I_n\left(\lambda_{nk}\,r\right) + C_{nk3}\,K_n\left(\lambda_{nk}\,r\right)\right]\right.$$

$$\left. \times\left[\beta_{ns}\tanh\left(\beta_{ns}\,L\right)F_{ns}\right]^{-1}\sum_{m=1}^{M}q_{nm}\,\Pi_{nms}\left[Y_n\left(\beta_{ns}\,H\right)J_n\left(\beta_{ns}\,r\right) - J_n\left(\beta_{ns}\,H\right)Y_n\left(\beta_{ns}\,r\right)\right]dr\right\} \tag{59}$$

Therefore, Eq. (59) can be replaced by the simplified expression.

$$U_F^* = \frac{1}{2}\rho_o\,\kappa_\theta \sum_{s=1}^{\infty}\left[\beta_{ns}\tanh\left(\beta_{ns}\,L\right)F_{ns}\right]^{-1}\sum_{k=1}^{M}q_{nk}\,\Pi_{nks}\sum_{m=1}^{M}q_{nm}\,\Pi_{nms} \tag{60}$$

For Case D, the reference liquid kinetic energy, U_F^* in Eq. (52) is similarly given as

$$U_F^* = \frac{1}{2}\rho_o\,\kappa_\theta \sum_{s=1}^{\infty}\sum_{k=1}^{M}\left\{\int_a^R r\left[J_n\left(\lambda_{nk}\,r\right) + C_{nk1}\,Y_n\left(\lambda_{nk}\,r\right) + C_{nk2}\,I_n\left(\lambda_{nk}\,r\right) + C_{nk3}\,K_n\left(\lambda_{nk}\,r\right)\right]\right.$$

$$\left. \times\left[\beta_{ns}\tanh\left(\beta_{ns}\,L\right)Q_{ns}\right]^{-1}\sum_{m=1}^{M}q_{nm}\,\Delta_{nms}\,J_n\left(\beta_{ns}\,r\right)dr\right\} \tag{61}$$

Therefore, Eq. (61) can be compactly written as

$$U_F^* = \frac{1}{2}\rho_o\,\kappa_\theta \sum_{s=1}^{\infty}\left[\beta_{ns}\tanh\left(\beta_{ns}\,L\right)Q_{ns}\right]^{-1}\sum_{k=1}^{M}q_{nk}\,\Delta_{nks}\sum_{m=1}^{M}q_{nm}\,\Delta_{nms} \tag{62}$$

A sufficiently large finite number, M in Eqs. (56), (58), (60) and (62) can guarantee the converged solution in the expanding the terms m and k to perform the numerical calculations for each circumferential wave number, n. The summation of s is also stopped for numerical computation, at a large integer value to acquire the required accuracy. It can be assumed that the liquid edge radius, H is large enough to converge the solution for simmulation of the radially unbounded infinite liquid.

A column vector, q of the unknown coefficients in conjunction with the plate is introduced for numerical calculations.

$$q = \left\{q_{n1}\quad q_{n2}\quad q_{n3}\cdots q_{nM}\right\}^T \tag{63}$$

Upon applying Eq. (63) to Eqs. (56), (58), (60) and (62), the reference kinetic energy of the liquid can be written as a matrix form.

$$U_F^* = \rho_o\,\kappa_\theta\,q^T\,G\,q\,/\,2 \tag{64}$$

where the added virtual mass incremental (AVMI) matrix, G for the fixed n is obtained by integration in Eqs. (55), (57), (59) and (61) with respect to the four liquid boundary conditions. The reference kinetic energy of the annular plate is calculated using the orthogonal property of the dry mode shapes.

$$T_p^* = \rho \, \kappa_\theta \, q^T \, Z \, q \, / \, 2 \tag{65}$$

where Z is the reference kinetic energy matrix of the annular plate given as

$$Z_{ik} = h \, P_i \, \delta_{ik} \, / \, 2 \tag{66}$$

$$P_i = \int_a^R r \, (\bar{W}_{ni})^2 \, dr \, , \quad \delta_{ik} : \text{Kronecker delta } (i, k = 1, 2, 3 \dots M) \tag{67}$$

When Eq. (4) is substituted into Eq. (67), and integrated with respect to the variable r from a to R, we can obtain a simple expression for the reference kinetic energy of the annular plate. On the other hand, the maximum potential energy of the annular plate can be computed by Eq. (68).

$$V_d = \kappa_\theta \, q^T U \, q \, / \, 2 \tag{68}$$

where κ_θ is defined in Eq. (53) and U is the diagonal matrix given by

$$U_{ik} = \lambda_{ni}^2 \, D \, P_i \, \delta_{ik} \, / \, 2 \quad (i, k = 1, 2, 3 \dots M) \tag{69}$$

As delineated in Eqs. (50) and (51), the relationships between the reference kinetic energy and the maximum potential energy lead to an eigenvalue problem for the annular plate in contact with the liquid with various radial liquid boundary conditions (Amabili 1996, Jeong *et al.* 2009).

$$U \, q - \omega^2 \left(\rho \, Z + \rho_o \, G \right) q = \{ 0 \} \tag{70}$$

Consequently, the eigenvalus and the corresponding eigenvectors of Eq. (70) can be extracted.

4. Examples and discussion

4.1 Theoretical and finite element models

The determinant of Eq. (70) is calculated using the commercial software Mathcad (release15) to extract the natural frequencies of an annular plate in contact with a liquid. The theoretical calculation involves an infinite and a finite series of algebraic terms, but the expansion in the mode and the series expansion should be truncated for effective calculation. The expanding terms s and m are set at 100 and 40 to obtain converged solutions, respectively.

In addition to the theoretical calculation, finite element analyses are also carried out using a commercial computer software, ANSYS (release 18.2) to check the validity of the theoretical formulation with respect for four cases of the radial liquid boundary condition, with a liquid depth denoted as d=80 mm. Two-dimensional axisymmetric finite element models of a liquid-coupled annular plate are constructed with the same plate geometry, boundary conditions and material properties as used in the theoretical calculation. The input data used in the theoretical calculations and the finite element analyses are listed in Table 1. The viscosity and compressibility of the liquid are ignored in both the theoretical calculations and the finite element analyses.

Table 1 Dimension and mechanical data of an annular plate in contact with a liquid

Component	Geometry and material property	Unit	Symbol	Value
Annular plate	Thickness	mm	h	2.0
	Outer radius	mm	R	200.0
	Inner radius	mm	a	50.0
	Mass density	kg/m^3	ρ	2700.0
	Modulus of elasticity	GPa	E	69.0
	Poisson's ratio	-	μ	0.33
	Outer container radius	mm	R	200.0
	Inner cylinder radius	mm	a	50.0
	Liquid outer edge radius	mm	H	2000.0
Liquid	Mass density	kg/m^3	ρ_o	1000.0
	Depth	mm	L	80.0

The axisymmetric models in the finite element analyses consist of axisymmetric harmonic liquid elements (FLUID81) and axisymmetric harmonic shell elements (SHELL61). The liquid domain is divided into a number of identical fluid elements, and the annular plate is also divided into identical shell elements. The nodes of the fluid elements at $r=0$ are constrained in the radial direction only for Case A and Case D. At the same time, the liquid movement at $r=R$, namely along the rigid outer cylindrical container, is also restricted to the radial direction to simulate Eq. (14) for Case A. In Case B, all nodes of the fluid elements at both $r=a$ and $r=R$ are radially restricted to attain the constraints along both the inner rigid cylinder and the outer rigid container as specified in Eqs. (16) and (17). In Case C, the nodes of the fluid elements at $r=a$ are only constrained in the radial direction to achieve the liquid boundary condition of the inner rigid cylinder wall as written in Eq. (20). On the other hand, the radial boundary at the outer edge of the liquid domain is not restricted to simulate Eq. (21) for Case C. For Case D, the boundary at the outer edge of the liquid domain is also unrestricted to simulate Eq. (21).

The vertical displacement of all nodes at the rigid bottom surface is limited for all cases to satisfy Eq. (11). The vertical displacement of all nodes in the liquid element adjacent to each surface of the wetted annular plate coincides with that of the plate elements so that the finite element model can simulate the compatibility requirement of Eq. (25). The flexible annular plate is divided into 60 two-dimensional axisymmetric shell elements with the same size for all the four cases. In addition, the liquid region of the finite element model with the liquid depth, $L=80$ mm, consists of 2560 (80×32) identical liquid elements for Case A, 1920 (60×32) liquid elements for Case B, 24960 (780×32) for Case C, and 25600 (800×32) for Case D. All the displacements and rotation are constrained along both plate edges in order to simulate the clamped boundary condition in the finite element analysis model. The 50 modal natural frequencies and mode shapes are extracted up to 18000 Hz using the Block Lanczos method in the finite element analyses.

4.2 Verification of analytical method

The theoretical and numerical natural frequencies of the wet annular plate are presented in Table 2 for Cases A, B, C and D, in the range of $0 \leq n \leq 3$ and $0 \leq m' \leq 3$. The symbol m' in Table 2 and Figs. 2-8 represents the number of nodal circles in a vibration mode. The theoretical natural frequencies agree well with the finite element results as shown in Table 2, verifying the proposed theory for

Table 2 Verification for natural frequencies of an annular plate in contact with a liquid

Mode no.*		Natural frequency (Hz)							
		Case A		Case B		Case C		Case D	
n	m'	Theory	ANSYS	Theory	ANSYS	Theory	ANSYS	Theory	ANSYS
0	1	490.1	491.6	491.8	489.6	501.9	502.1	501.3	501.2
	2	1335.1	1154.8	1337.6	1151.4	1168.0	1172.5	1172.1	1165.6
	3	2182.4	2249.4	2168.6	2239.4	2263.4	2258.3	2269.8	2282.2
1	0	104.0	104.2	94.0	94.2	114.8	114.9	122.4	122.4
	1	514.2	525.6	506.7	517.3	533.9	534.1	541.3	542.4
	2	1191.8	1221.9	1174.9	1200.3	1215.7	1228.1	1247.7	1247.5
	3	2220.4	2303.7	2192.3	2279.3	2308.6	2309.2	2328.3	2345.7
2	0	167.5	168.1	164.7	165.8	179.0	178.7	180.9	180.9
	1	581.0	595.3	576.1	589.8	609.8	609.8	615.4	615.6
	2	1282.8	1321.9	1275.4	1307.6	1352.7	1338.9	1351.6	1353.2
	3	2318.3	2408.4	2289.2	2387.1	2422.9	2425.8	2443.2	2447.3
3	0	242.7	244.7	241.1	244.1	253.5	253.7	254.3	254.3
	1	685.2	703.0	682.1	701.2	719.7	720.4	723.1	723.3
	2	1422.1	1461.5	1418.1	1453.4	1463.2	1483.8	1491.2	1492.1
	3	2462.4	2565.1	2432.0	2550.2	2584.0	2590.8	2603.8	2605.9

*n=Number of nodal diameter, m'=Number of nodal circles
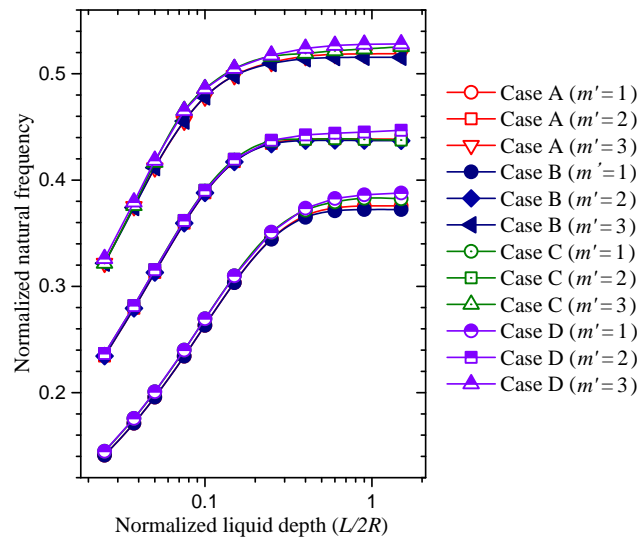
Fig. 2 Normalized natural frequencies of a liquid contacting annular plate for $n=0$

Cases A, B, C and D by the finite element analyses. The maximum discrepancy between the theoretical and finite element results tends to increase with mode numbers as demonstrated in Table 2. The axisymmetric mode with $n=0$ and $m'=0$ is not included in the Table 2 because the specific mode violates the liquid volume conservation, as explained in a previous study (Jeong *et al.* 2005).
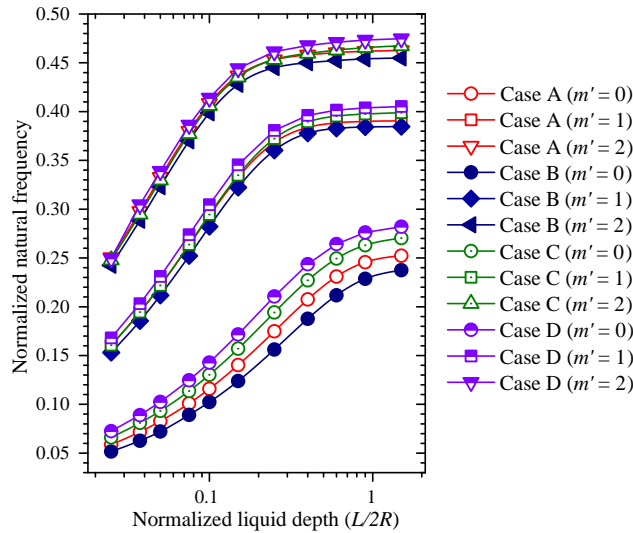
Fig. 3 Normalized natural frequencies of a liquid contacting annular plate for *n*=1
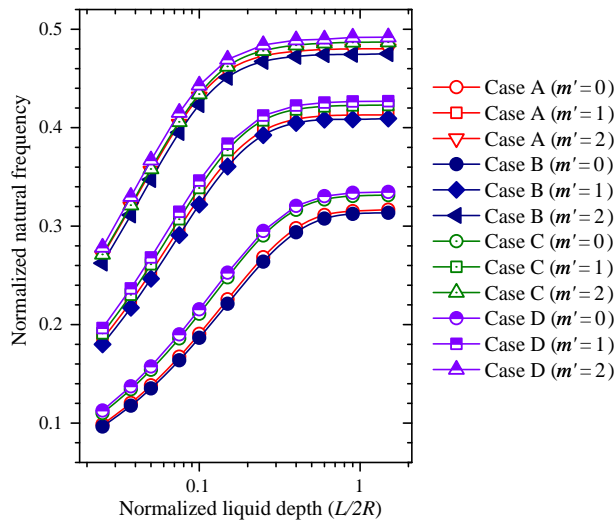

Fig. 4 Normalized natural frequencies of a liquid contacting annular plate for *n*=2

4.3 Effect of liquid boundary condition

The natural frequency of a structure in contact with a liquid is well known to be lower than the corresponding natural frequency in air due to the hydrodynamic mass effect on the structure's motion. Hence, the normalized natural frequency, defined as the natural frequency of the wet annular plate divided by the corresponding natural frequency of the dry annular plate, ranges between unity and zero regardless of the mode, as demonstrated in Figs. 2-4. The normalized natural frequencies are plotted in Figs. 2-4 as a function of normalized liquid depth, *L/2R*, for *n*=0, 1, and 2, respectively.

A reduction in the liquid depth significantly affects the wet natural frequencies when approximately *L<R*. As the liquid depth *L* decreases, the hydrodynamic mass amplifies and reduces

(a) $n=0$, $m'=1$ (b) $n=0$, $m'=2$

(c) $n=1$, $m'=0$ (d) $n=1$, $m'=1$
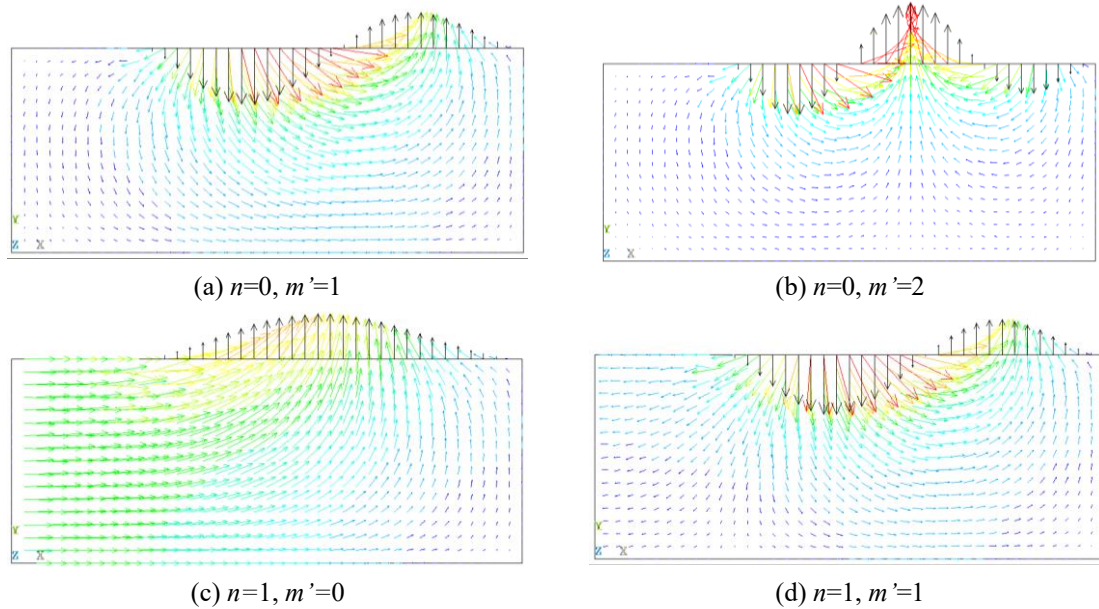
Fig. 5 Vector plots of mode shape in a liquid-contacting annular plate for Case A

the natural frequency of the wet annular plate. The natural frequencies increase drastically with increasing liquid depth, regardless of the radial boundary condition of the liquid, and eventually converge to those of the annular plate floating on an infinite liquid depth. The wet natural frequency of the liquid-coupled annular plate primarily depends on the total moving liquid volume during vibration. Therefore, the effect of liquid depth on the wet natural frequencies is more dominant than the influence of the radial liquid constraints. It is obvious that an increase in the number of nodal circles, m' or nodal diameter, n reduces the hydrodynamic mass, and increases wet natural frequencies due to the separation effect in the liquid flow. As the number of nodal circles, m', and nodal diameter, n, increases, the oscillating liquid regions become more divided.

Figs. 5-8 depict the deflection vectors of both the annular plate and the contained liquid for Cases A, B, C and D, with respect to $n=0$, 1 and $m'=0$, 1, 2. Figs. 2-8 reveal that the effect of the radial liquid boundary condition on the natural frequencies and the mode shapes is relatively insignificant. However, upon closer examination of the difference in the wet natural frequencies for the four cases of the radial liquid boundary condition, it is observed that the natural frequencies of the liquid-coupled plate depend on the radial liquid boundary condition for certain vibrational modes. Roughly speaking, the normalized natural frequencies of the axisymmetric mode with $n=0$ do not depend on the radial liquid boundary conditions as shown in Fig. 2. This is because the liquid motions at the inner cylinder region of Case A and Case D are relatively small as illustrated in the vector plots for $n=0$ in Figs. 5-8. In other words, the difference between the liquid vectors of the four cases is negligible, which means that the inner cylinder and the outer container do not affect the mode shapes and wet natural frequencies for the axisymmetric mode $n=0$.

On the other hand, the normalized natural frequencies with $n=1$ and $n=2$ considerably depend on the radial liquid boundary conditions for $m'=0$ as shown in Figs. 3 and 4 because the liquid motions at the inner cylinder region of Case A and the outer container region of Case C are relatively significant as illustrated in the vector plots of Fig. 5(c) and Fig. 7(c). As the radial movement of
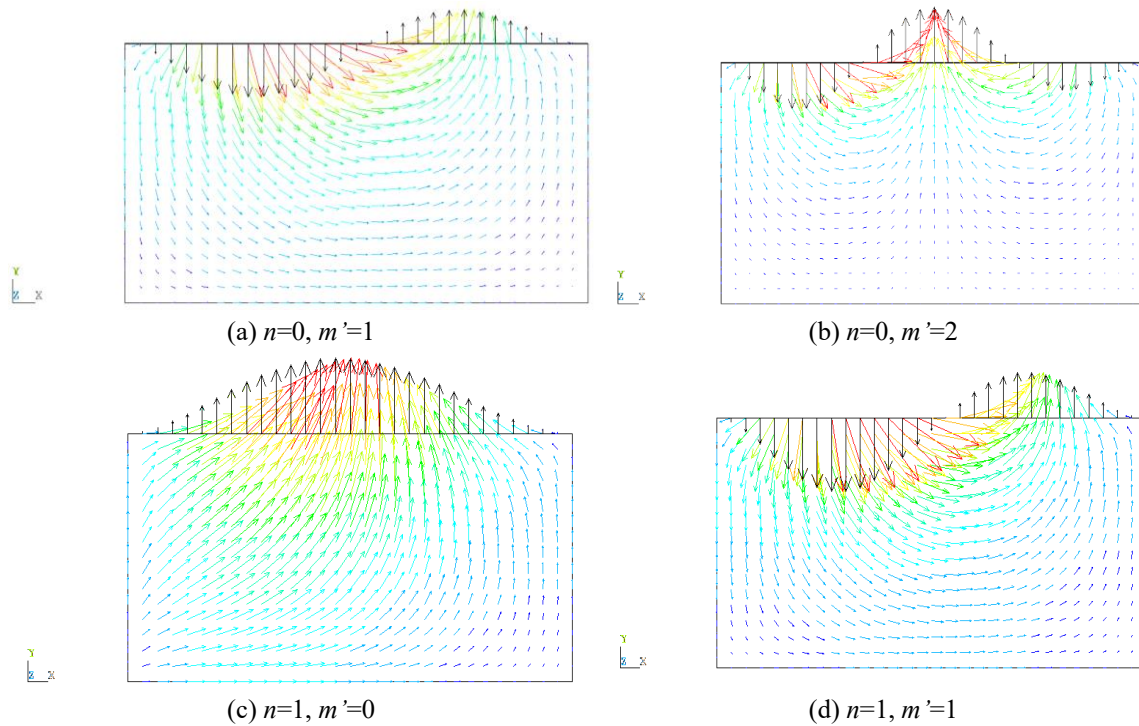
(a) $n=0$, $m'=1$

(b) $n=0$, $m'=2$

(c) $n=1$, $m'=0$

(d) $n=1$, $m'=1$

Fig. 6 Vector plots of mode shape in a liquid-contacting annular plate for Case B

liquid across the centerline of the cylinder is allowed for $n=1$, the effect of the radial constraints such as the cylinder and container becomes relatively significant. The difference in the normalized natural frequency between the radial liquid boundary conditions is clearly demonstrated in Figs. 3 and 4.

Furthermore, the presence of the inner rigid cylinder and the outer rigid container also increases the hydrodynamic mass, leading to a reduction in the fundamental natural frequency for the circumferential mode $n=1$. The natural frequencies of Case B are lower than those of Case A, and the natural frequencies of Case A are lower than those of Case C regardless of mode numbers as listed in Table 2. It is evident that the any solid obstacles, such as the rigid wall of the inner cylinder or the outer container, increase the hydrodynamic mass and reduce the natural frequencies. This tendency is prominent for the specific mode number with $n=1$ and $m'=0$, as the radial liquid movement is maximized in this mode.

5. Conclusions

This paper presents an analytical method for analyzing the free vibration of a liquid-contacting annular plate considering, whether or not the contained liquid is constrained by a rigid inner cylinder or outer container. The displacement potential functions that satisfy the Laplace equation and liquid boundary conditions are obtained to describe the liquid motions. The fluid-structure coupling at the interface between the annular plate and the liquid is taken into account. The wet dynamic displacement of the annular plate is expressed as a combination of dry modal functions, and the
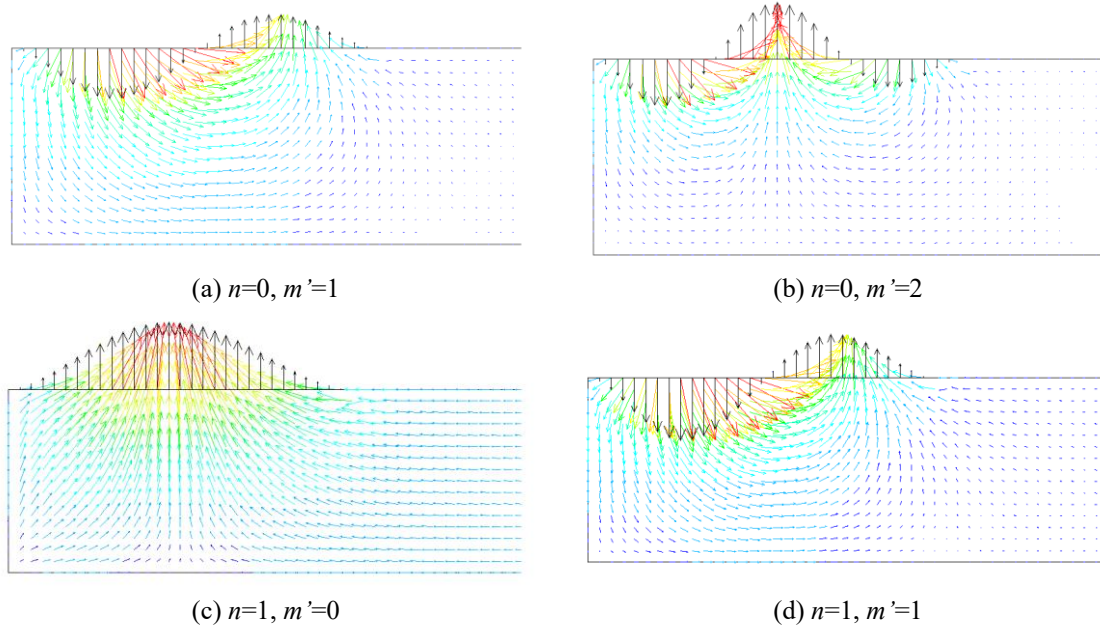
(a) *n*=0, *m'*=1   (b) *n*=0, *m'*=2

(c) *n*=1, *m'*=0   (d) *n*=1, *m'*=1

Fig. 7 Vector plots of mode shape in a liquid-contacting annular plate for Case C

(a) *n*=0, *m'*=1   (b) *n*=0, *m'*=2

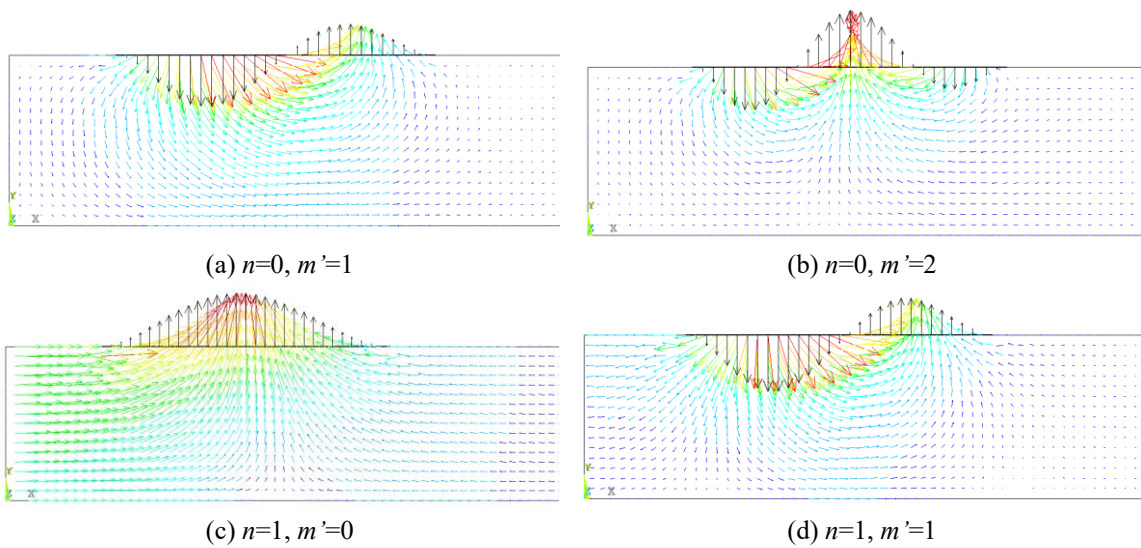(c) *n*=1, *m'*=0   (d) *n*=1, *m'*=1

Fig. 8 Vector plots of mode shape in a liquid-contacting annular plate for Case D

Rayleigh-Ritz method is applied to derive a matrix equation for extracting the natural frequencies of the system. The effect of radial liquid boundary conditions on the dynamic characteristics of the system is investigated for four cases: the outer bounded liquid case, the outer and inner bounded liquid case, the inner bounded liquid case, and the radially unbounded case. The accuracy of the theoretical formulation is validated by comparing the results with the finite element analysis. It is found that the radial liquid bounding effect on the natural frequencies is negligible for the

axisymmetric vibrational mode, but becomes relatively significant for the mode with $n=1$ and $m'=0$. Furthermore, the study reveals that the hydrodynamic mass is largest for the outer and inner bounded liquid case, regardless of the vibration mode.

Acknowledgement

References

Amabili, M. (1996), "Effect of finite fluid depth on the hydroelastic vibrations of circular and annular plates", *J. Sound Vib.*, **193**(4), 909-925. https://doi.org/10.1006/jsvi.1996.0322.

Amabili, M., Frosali, G. and Kwak, M.K. (1996), "Free vibrations of annular plates coupled with fluids", *J. Sound Vib.*, **191**(5), 825-846. https://doi.org/10.1006/jsvi.1996.0158.

Askari, E., Jeong, K.H. and Amabili, M. (2013), "Hydroelastic vibration of circular plates immersed in a liquid-filled container with free surface", *J. Sound Vib.*, **332**(12), 3064-3085. https://doi.org/10.1016/j.jsv.2013.01.007.

Askari, E., Jeong, K.H., Ahn, K.H. and Amabili, M. (2020), "A mathematical approach to study fluid-coupled vibration of eccentric annular plates", *J. Fluid. Struct.*, **98**, 103129. https://doi.org/10.1016/j.jfluidstructs.2020.103129.

Bauer, H. and Komatsu, K. (2000), "Coupled frequencies of a frictionless liquid in a circular cylindrical tank with an elastic partial surface cover", *J. Sound Vib.*, **230**(5), 1147-1163. https://doi.org/10.1006/jsvi.1999.2662.

Chen, G.W., Liao, C.Y., Lin, Y.Z. and Ma, C.C. (2021), "Analytic solution to the coupled characteristics of a rectangular plate partially immersed in a finite fluid container", *J. Sound Vib.*, **515**, 116446. https://doi.org/10.1016/j.jsv.2021.116446.

Escaler, X. and De La Torre, O. (2018), "Axisymmetric vibrations of a circular Chladni plate in air and fully submerged in water", *J. Fluid. Struct.*, **82**, 432-445. https://doi.org/10.1016/j.jfluidstructs.2018.07.017.

Hosseini, M., Goudarzi. M.A. and Soroor. A. (2017), "Reduction of seismic sloshing in floating roof liquid storage tanks by using a suspended annular baffle", *J. Fluid. Struct.*, **71**, 40-55. http://dx.doi.org/10.1016/j.jfluidstructs.2017.02.008.

Jeong, K.H. (2006), "Hydroelastic vibration of two annular plates coupled with a bounded compressible fluid", *J. Fluid. Struct.*, **22**(8), 1079-1096. https://doi.org/10.1016/j.jfluidstructs.2006.07.001.

Jeong, K.H. and Kim, K.J. (2005), "Hydroelastic vibration of a circular plate submerged in a bounded compressible fluid", *J. Sound Vib.*, **283**(1-2), 153-172. https://doi.org/10.1016/j.jsv.2004.04.029.

Kim, Y.W. and Lee, Y.S. (2005), "Coupled vibration analysis of liquid-filled rigid cylindrical storage tank with an annular plate cover", *J. Sound Vib.*, **279**(1-2), 217-235. https://doi.org/10.1016/j.jsv.2003.10.032.

Kwak, M.K. and Amabili, M. (1999), "Hydroelastic vibration of free-edge annular plates", *ASME J. Vib. Acoust.*, **121**, 26-32. https://doi.org/10.1115/1.2893944.

Kwak, M.K. and Han, S.B. (2000), "Effect of fluid depth on the hydroelastic vibration of free-edge circular plate", *J. Sound Vib.*, **230**(1), 171-185. https://doi.org/10.1006/jsvi.1999.2608.

Liang, C.C., Tai, Y.S. and Li, P.L. (1999), "Natural frequencies of annular plates having contact with fluid", *J. Sound Vib.*, **228**(5), 1167-1181. https://doi.org/10.1006/jsvi.1999.2463.

Lin, G.Z., Yang, Y., He, Z.G. and Jiao, P.C. (2022), "Hydrodynamic optimization in high-acceleration underwater motions using added-mass coefficient", *Ocean Eng.*, **263**, 112274. https://doi.org/10.1016/j.oceaneng.2022.112274.

Wang, P.G., Zhao, M. and Du, X.L. (2019), "A simple added mass model for simulating elliptical cylinder vibrating in water under earthquake action", *Ocean Eng.*, **179**, 351-360. https://doi.org/10.1016/j.oceaneng.2019.02.046.

Zhang, J.R., Wei, K. and Qin, S.Q. (2022), "An efficient numerical model for hydrodynamic added mass of immersed column with arbitrary cross section", *Ocean Eng.*, **187**, 106192. https://doi.org/10.1016/j.oceaneng.2019.106192.

CC

Appendix

1. Mode shapes coefficients of clamped annular plate

$$C_{nm1} = \frac{1}{T_{nm}}\left[\left\{ I^{da}_{nm}\,K^{R}_{nm} - I^{R}_{nm}\,K^{da}_{nm} \right\} J^{a}_{nm} + \left\{ I^{a}_{nm}\,K^{da}_{nm} - I^{da}_{nm}\,K^{a}_{nm} \right\} J^{R}_{nm} + \left\{ I^{R}_{nm}\,K^{a}_{nm} - I^{a}_{nm}\,K^{R}_{nm} \right\} J^{da}_{nm}\right],$$

$$C_{nm2} = \frac{1}{T_{nm}}\left[\left\{ Y^{R}_{nm}\,K^{da}_{nm} - Y^{da}_{nm}\,K^{R}_{nm} \right\} J^{a}_{nm} + \left\{ Y^{da}_{nm}\,K^{a}_{nm} - Y^{a}_{nm}\,K^{da}_{nm} \right\} J^{R}_{nm} + \left\{ Y^{a}_{nm}\,K^{R}_{nm} - Y^{R}_{nm}\,K^{a}_{nm} \right\} J^{da}_{nm}\right],$$

$$C_{nm3} = \frac{1}{T_{nm}}\left[\left\{ I^{R}_{nm}\,Y^{da}_{nm} - I^{da}_{nm}\,Y^{R}_{nm} \right\} J^{a}_{nm} + \left\{ I^{da}_{nm}\,Y^{a}_{nm} - I^{a}_{nm}\,Y^{da}_{nm} \right\} J^{R}_{nm} + \left\{ I^{a}_{nm}\,Y^{R}_{nm} - I^{R}_{nm}\,Y^{a}_{nm} \right\} J^{da}_{nm}\right],$$

$$T_{nm} = \left(I^{R}_{nm}\,K^{da}_{nm} - I^{da}_{nm}\,K^{R}_{nm} \right) Y^{a}_{nm} - \left(I^{R}_{nm}\,K^{a}_{nm} - I^{a}_{nm}\,K^{R}_{nm} \right) Y^{da}_{nm} + \left(I^{da}_{nm}\,K^{a}_{nm} - I^{a}_{nm}\,K^{da}_{nm} \right) Y^{R}_{nm},$$

$$J^{a}_{nm} = J_{n}(\lambda_{nm}a),\quad J^{da}_{nm} = J_{n}{}'(\lambda_{nm}a),\quad J^{R}_{nm} = J_{n}(\lambda_{nm}R),\quad J^{dR}_{nm} = J_{n}{}'(\lambda_{nm}R),$$

$$Y^{a}_{nm} = Y_{n}(\lambda_{nm}a),\quad Y^{da}_{nm} = Y_{n}{}'(\lambda_{nm}a),\quad Y^{R}_{nm} = Y_{n}(\lambda_{nm}R),\quad Y^{dR}_{nm} = Y_{n}{}'(\lambda_{nm}R),$$

$$I^{a}_{nm} = I_{n}(\lambda_{nm}a),\quad I^{da}_{nm} = I_{n}{}'(\lambda_{nm}a),\quad I^{R}_{nm} = I_{n}(\lambda_{nm}R),\quad I^{dR}_{nm} = I_{n}{}'(\lambda_{nm}R),$$

$$K^{R}_{nm} = K_{n}(\lambda_{nm}R),\quad K^{da}_{nm} = K_{n}{}'(\lambda_{nm}a),\quad K^{R}_{nm} = K_{n}(\lambda_{nm}R),\quad K^{dR}_{nm} = K_{n}{}'(\lambda_{nm}R)$$

2. Integral coefficients

Case A

$$\Gamma_{nms1} = \xi_{nms1}\left[(\lambda_{nm}R)\,\sigma^{R}_{ns}\,J^{dR}_{nm} - (\lambda_{nm}a)\,\sigma^{a}_{ns}\,J^{da}_{nm} + (\beta_{ns}a)\,J^{a}_{nm}\,\sigma^{da}_{ns} \right],$$

$$\Gamma_{nms2} = \xi_{nms1}\left[(\lambda_{nm}R)\,\sigma^{R}_{ns}\,Y^{dR}_{nm} - (\lambda_{nm}a)\,\sigma^{a}_{ns}\,Y^{da}_{nm} + (\beta_{ns}a)\,Y^{a}_{nm}\,\sigma^{da}_{ns} \right],$$

$$\Gamma_{nms3} = \xi_{nms2}\left[(\lambda_{nm}R)\,\sigma^{R}_{ns}\,I^{dR}_{nm} - (\lambda_{nm}a)\,\sigma^{a}_{ns}\,I^{da}_{nm} + (\beta_{ns}a)\,I^{a}_{nm}\,\sigma^{da}_{ns} \right],$$

$$\Gamma_{nms4} = \xi_{nms2}\left[(\lambda_{nm}R)\,\sigma^{R}_{ns}\,K^{dR}_{nm} - (\lambda_{nm}a)\,\sigma^{a}_{ns}\,K^{da}_{nm} + (\beta_{ns}a)\,K^{a}_{nm}\,\sigma^{da}_{ns} \right],\quad E_{ns} = R^{2}\,\varsigma^{R}_{ns}\,(\sigma^{R}_{ns})^{2}/2$$

Case B

$$\Lambda_{nms1} = \tau^{dR}_{ns}\,\xi_{nms1}\left[(\lambda_{nm}R)\,\sigma^{R}_{ns}\,J^{dR}_{nm} - (\beta_{ns}R)\,J^{R}_{nm}\,\sigma^{dR}_{ns} - (\lambda_{nm}a)\,\sigma^{a}_{ns}\,J^{da}_{nm} + (\beta_{ns}a)\,J^{a}_{nm}\,\sigma^{da}_{ns} \right]$$
$$- \sigma^{dR}_{ns}\,\xi_{nms1}\left[(\lambda_{nm}R)\,\tau^{R}_{ns}\,J^{dR}_{nm} - (\beta_{ns}R)\,J^{R}_{nm}\,\tau^{dR}_{ns} - (\lambda_{nm}a)\,\tau^{a}_{ns}\,J^{da}_{nm} + (\beta_{ns}a)\,J^{a}_{nm}\,\tau^{da}_{ns} \right],$$

$$\Lambda_{nms2} = \tau^{dR}_{ns}\,\xi_{nms1}\left\{ (\lambda_{nm}R)\,\sigma^{R}_{ns}\,Y^{dR}_{nm} - (\beta_{ns}R)\,Y^{R}_{nm}\,\sigma^{dR}_{ns} - (\lambda_{nm}a)\,\sigma^{a}_{ns}\,Y^{da}_{nm} + (\beta_{ns}a)\,Y^{a}_{nm}\,\sigma^{da}_{ns} \right\}$$
$$- \sigma^{dR}_{ns}\,\xi_{nms1}\left\{ (\lambda_{nm}R)\,\tau^{R}_{ns}\,Y^{dR}_{nm} - (\beta_{ns}R)\,Y^{R}_{nm}\,\tau^{dR}_{ns} - (\lambda_{nm}a)\,\tau^{a}_{ns}\,Y^{da}_{nm} + (\beta_{ns}a)\,Y^{a}_{nm}\,\tau^{da}_{ns} \right\},$$

$$\Lambda_{nms3} = \tau^{dR}_{ns}\,\xi_{nms2}\left\{ (\lambda_{nm}R)\,\sigma^{R}_{ns}\,I^{dR}_{nm} - (\beta_{ns}R)\,I^{R}_{nm}\,\sigma^{dR}_{ns} - (\lambda_{nm}a)\,\sigma^{a}_{ns}\,I^{da}_{nm} + (\beta_{ns}a)\,I^{a}_{nm}\,\sigma^{da}_{ns} \right\}$$
$$- \sigma^{dR}_{ns}\,\xi_{nms2}\left\{ (\lambda_{nm}R)\,\tau^{R}_{ns}\,I^{dR}_{nm} - (\beta_{ns}R)\,I^{R}_{nm}\,\tau^{dR}_{ns} - (\lambda_{nm}a)\,\tau^{a}_{ns}\,I^{da}_{nm} + (\beta_{ns}a)\,I^{a}_{nm}\,\tau^{da}_{ns} \right\},$$

$$\Lambda_{nms4} = \tau^{dR}_{ns}\,\xi_{nms2}\left\{ (\lambda_{nm}R)\,\sigma^{R}_{ns}\,K^{dR}_{nm} - (\beta_{ns}R)\,K^{R}_{nm}\,\sigma^{dR}_{ns} - (\lambda_{nm}a)\,\sigma^{a}_{ns}\,K^{da}_{nm} + (\beta_{ns}a)\,K^{a}_{nm}\,\sigma^{da}_{ns} \right\}$$
$$- \sigma^{dR}_{ns}\,\xi_{nms2}\left\{ (\lambda_{nm}R)\,\tau^{R}_{ns}\,K^{dR}_{nm} - (\beta_{ns}R)\,K^{R}_{nm}\,\tau^{dR}_{ns} - (\lambda_{nm}a)\,\tau^{a}_{ns}\,K^{da}_{nm} + (\beta_{ns}a)\,K^{a}_{nm}\,\tau^{da}_{ns} \right\},$$

$$G_{ns} = R^2 \left[(\sigma_{ns}^{dR})^2 (\tau_{ns}^{dR})^2 + \frac{1}{2} \varsigma_{ns}^R \left\{ (\sigma_{ns}^R)^2 (\tau_{ns}^{dR})^2 + (\sigma_{ns}^{dR})^2 (\tau_{ns}^R)^2 \right\} \right]$$

$$- a^2 \left[(\sigma_{ns}^{dR})^2 (\tau_{ns}^{da})^2 + \frac{1}{2} \varsigma_{ns}^a \left\{ (\sigma_{ns}^a)^2 (\tau_{ns}^{dR})^2 + (\sigma_{ns}^{dR})^2 (\tau_{ns}^a)^2 \right\} \right]$$

Case C

$$\Xi_{nms1} = \tau_{ns}^H \, \xi_{nms1} \left[(\lambda_{nm} R) \, \sigma_{ns}^R \, \mathrm{J}_{nm}^{dR} - (\beta_{ns} R) \, \mathrm{J}_{nm}^R \, \sigma_{ns}^{dR} - (\lambda_{nm} a) \, \sigma_{ns}^a \, \mathrm{J}_{nm}^{da} + (\beta_{ns} a) \, \mathrm{J}_{nm}^a \, \sigma_{ns}^{da} \right]$$

$$- \sigma_{ns}^H \, \xi_{nms1} \left[(\lambda_{nm} R) \, \tau_{ns}^R \, \mathrm{J}_{nm}^{dR} - (\beta_{ns} R) \, \mathrm{J}_{nm}^R \, \tau_{ns}^{dR} - (\lambda_{nm} a) \, \tau_{ns}^a \, \mathrm{J}_{nm}^{da} + (\beta_{ns} a) \, \mathrm{J}_{nm}^a \, \tau_{ns}^{da} \right],$$

$$\Xi_{nms2} = \tau_{ns}^H \, \xi_{nms1} \left[(\lambda_{nm} R) \, \sigma_{ns}^R \, \mathrm{Y}_{nm}^{dR} - (\beta_{ns} R) \, \mathrm{Y}_{nm}^R \, \sigma_{ns}^{dR} - (\lambda_{nm} a) \, \sigma_{ns}^a \, \mathrm{Y}_{nm}^{da} + (\beta_{ns} a) \, \mathrm{Y}_{nm}^a \, \sigma_{ns}^{da} \right]$$

$$- \sigma_{ns}^H \, \xi_{nms1} \left[(\lambda_{nm} R) \, \tau_{ns}^R \, \mathrm{Y}_{nm}^{dR} - (\beta_{ns} R) \, \mathrm{Y}_{nm}^R \, \tau_{ns}^{dR} - (\lambda_{nm} a) \, \tau_{ns}^a \, \mathrm{Y}_{nm}^{da} + (\beta_{ns} a) \, \mathrm{Y}_{nm}^a \, \tau_{ns}^{da} \right],$$

$$\Xi_{nms3} = \tau_{ns}^H \, \xi_{nms2} \left[(\lambda_{nm} R) \, \sigma_{ns}^R \, \mathrm{I}_{nm}^{dR} - (\beta_{ns} R) \, \mathrm{I}_{nm}^R \, \sigma_{ns}^{dR} - (\lambda_{nm} a) \, \sigma_{ns}^a \, \mathrm{I}_{nm}^{da} + (\beta_{ns} a) \, \mathrm{I}_{nm}^a \, \sigma_{ns}^{da} \right]$$

$$- \sigma_{ns}^H \, \xi_{nms2} \left[(\lambda_{nm} R) \, \tau_{ns}^R \, \mathrm{I}_{nm}^{dR} - (\beta_{ns} R) \, \mathrm{I}_{nm}^R \, \tau_{ns}^{dR} - (\lambda_{nm} a) \, \tau_{ns}^a \, \mathrm{I}_{nm}^{da} + (\beta_{ns} a) \, \mathrm{I}_{nm}^a \, \tau_{ns}^{da} \right],$$

$$\Xi_{nms4} = \tau_{ns}^H \, \xi_{nms2} \left[(\lambda_{nm} R) \, \sigma_{ns}^R \, \mathrm{K}_{nm}^{dR} - (\beta_{ns} R) \, \mathrm{K}_{nm}^R \, \sigma_{ns}^{dR} - (\lambda_{nm} a) \, \sigma_{ns}^a \, \mathrm{K}_{nm}^{da} + (\beta_{ns} a) \, \mathrm{K}_{nm}^a \, \sigma_{ns}^{da} \right]$$

$$- \sigma_{ns}^H \, \xi_{nms2} \left[(\lambda_{nm} R) \, \tau_{ns}^R \, \mathrm{K}_{nm}^{dR} - (\beta_{ns} R) \, \mathrm{K}_{nm}^R \, \tau_{ns}^{dR} - (\lambda_{nm} a) \, \tau_{ns}^a \, \mathrm{K}_{nm}^{da} + (\beta_{ns} a) \, \mathrm{K}_{nm}^a \, \tau_{ns}^{da} \right],$$

$$F_{ns} = \frac{(\tau_{ns}^H)^2}{2} \left[H^2 \left\{ (\sigma_{ns}^{dH})^2 + \varsigma_{ns}^H (\sigma_{ns}^H)^2 \right\} - a^2 \left\{ (\sigma_{ns}^{da})^2 + \varsigma_{ns}^a (\sigma_{ns}^a)^2 \right\} \right]$$

$$- \sigma_{ns}^H \, \tau_{ns}^H \left[H^2 \left(\sigma_{ns}^{dH} \, \tau_{ns}^{dH} + \varsigma_{ns}^H \, \sigma_{ns}^H \, \tau_{ns}^H \right) - a^2 \left(\sigma_{ns}^{da} \, \tau_{ns}^{da} + \varsigma_{ns}^a \, \sigma_{ns}^a \, \tau_{ns}^a \right) \right]$$

$$+ \frac{(\sigma_{ns}^H)^2}{2} \left[H^2 \left\{ (\tau_{ns}^{dH})^2 + \varsigma_{ns}^H (\tau_{ns}^H)^2 \right\} - a^2 \left\{ (\tau_{ns}^{da})^2 + \varsigma_{ns}^a (\tau_{ns}^a)^2 \right\} \right]$$

Case D

$$\Omega_{nms1} = \xi_{nms1} \left\{ R^2 \left[(\beta_{ns} R) \, \sigma_{ns}^{dR} \, \mathrm{J}_{nm}^R - (\lambda_{nm} R) \, \sigma_{ns}^R \, \mathrm{J}_{nm}^{dR} \right] + a^2 \left[(\lambda_{nm} a) \, \sigma_{ns}^a \, \mathrm{J}_{nm}^{da} - (\beta_{ns} a) \, \sigma_{ns}^{da} \, \mathrm{J}_{nm}^a \right] \right\},$$

$$\Omega_{nms2} = \xi_{nms1} \left\{ R^2 \left[(\beta_{ns} R) \, \sigma_{ns}^{dR} \, \mathrm{Y}_{nm}^R - (\lambda_{nm} R) \, \sigma_{ns}^R \, \mathrm{Y}_{nm}^{dR} \right] + a^2 \left[(\lambda_{nm} a) \, \sigma_{ns}^a \, \mathrm{Y}_{nm}^{da} - (\beta_{ns} a) \, \sigma_{ns}^{da} \, \mathrm{Y}_{nm}^a \right] \right\},$$

$$\Omega_{nms3} = \xi_{nms2} \left\{ R^2 \left[(\beta_{ns} R) \, \sigma_{ns}^{dR} \, \mathrm{I}_{nm}^R + (\lambda_{nm} R) \, \sigma_{ns}^R \, \mathrm{I}_{nm}^{dR} \right] + a^2 \left[(\lambda_{nm} a) \, \sigma_{ns}^a \, \mathrm{I}_{nm}^{da} + (\beta_{ns} a) \, \sigma_{ns}^{da} \, \mathrm{I}_{nm}^a \right] \right\},$$

$$\Omega_{nms4} = \xi_{nms2} \left\{ R^2 \left[(\beta_{ns} R) \, \sigma_{ns}^{dR} \, \mathrm{K}_{nm}^R + (\lambda_{nm} R) \, \sigma_{ns}^R \, \mathrm{K}_{nm}^{dR} \right] + a^2 \left[(\lambda_{nm} a) \, \sigma_{ns}^a \, \mathrm{K}_{nm}^{da} + (\beta_{ns} a) \, \sigma_{ns}^{da} \, \mathrm{K}_{nm}^a \right] \right\},$$

$$Q_{ns} = (\tau_{ns}^H)^2 H^2 (\sigma_{ns}^{dH})^2 / 2 ,$$

$$\xi_{nms1} = \frac{1}{\beta_{ns}^2 - \lambda_{nm}^2} , \quad \xi_{nms2} = \frac{1}{\beta_{ns}^2 + \lambda_{nm}^2} , \quad \varsigma_{ns}^R = 1 - \frac{n^2}{(\beta_{ns} R)^2} , \quad \varsigma_{ns}^a = 1 - \frac{n^2}{(\beta_{ns} a)^2} , \quad \varsigma_{ns}^H = 1 - \frac{n^2}{(\beta_{ns} H)^2} ,$$

$$\sigma_{ns}^R = \mathrm{J}_n (\beta_{ns} R) , \quad \sigma_{ns}^{dR} = \mathrm{J}_n'(\beta_{ns} R) , \quad \sigma_{ns}^a = \mathrm{J}_n (\beta_{ns} a) , \quad \sigma_{ns}^{da} = \mathrm{J}_n'(\beta_{ns} a) , \quad \sigma_{ns}^H = \mathrm{J}_n (\beta_{ns} H) ,$$

$$\sigma_{ns}^{dH} = \mathrm{J}_n'(\beta_{ns} H) ,$$

$$\tau_{ns}^{R} = Y_n(\beta_{ns}R), \quad \tau_{ns}^{dR} = Y_n'(\beta_{ns}R), \quad \tau_{ns}^{a} = Y_n(\beta_{ns}a), \quad \tau_{ns}^{da} = Y_n'(\beta_{ns}a), \quad \tau_{ns}^{H} = Y_n(\beta_{ns}H),$$

$$\tau_{ns}^{dH} = Y_n'(\beta_{ns}H)$$